

Integrated analysis of energy transfers in elastic-wave turbulence

Naoto Yokoyama*

Department of Aeronautics and Astronautics, Kyoto University, Kyoto 615-8540, Japan

Masanori Takaoka†

Department of Mechanical Engineering, Doshisha University, Kyotanabe 610-0394, Japan

(Dated: September 29, 2018)

In elastic-wave turbulence, strong turbulence appears in small wave numbers while weak turbulence does in large wave numbers. Energy transfers in the coexistence of these turbulent states are numerically investigated in both of the Fourier space and the real space. An analytical expression of a detailed energy balance reveals from which mode to which mode energy is transferred in the triad interaction. Stretching energy excited by external force is transferred nonlocally and intermittently to large wave numbers as the kinetic energy in the strong turbulence. In the weak turbulence, the resonant interactions according to the weak turbulence theory produces cascading net energy transfer to large wave numbers. Because the system's nonlinearity shows strong temporal intermittency, the energy transfers are investigated at active and moderate phases separately. The nonlocal interactions in the Fourier space are characterized by the intermittent bundles of fibrous structures in the real space.

PACS numbers: 62.30.+d, 05.45.-a, 46.40.-f

I. INTRODUCTION

Investigation of energy transfers, which reveals how the nonlinear interactions redistribute energy among scales, is essential to understand turbulence dynamics. For the Navier–Stokes turbulence, the so-called K41 theory [1] for energy cascade is based on the locality of the energy transfer. Representing the Navier–Stokes equation in the Fourier space, we can investigate the scale-by-scale energy budget. The energy transfer is caused by a triad interaction in the Navier–Stokes turbulence. When the three wave-number vectors, \mathbf{k} , \mathbf{k}_1 and \mathbf{k}_2 , make a triad, $\mathbf{k} + \mathbf{k}_1 + \mathbf{k}_2 = \mathbf{0}$, in the incompressible fluid, the sum of the energies of the three wave-number modes is conserved. The energy conservation through this triad interactions is called detailed energy balance. The energy is transferred locally in the Fourier space, because the small wave-number mode plays a role only as a mediator [2, 3]. The relation is under serious study between the energy cascade in the Fourier space and the dynamics of real-space structures.

It is important also in wave turbulence to identify from which mode a wave-number mode in the inertial subrange obtains energy, and to which mode the wave-number mode gives energy. The energy transfer has not been fully understood yet, because we are less successful even in obtaining the analytical expression for it in such a way that is consistent with the energy conservation. When the nonlinearity of wave turbulence is weak, the weak turbulence theory well describes the transfer of the linear energy, which is conserved by the kinetic equation. Even then, the detailed energy balance at each scale has never

been investigated. The difficulty comes in identifying the energy transfer between two wave-number modes in the interactions among three, four or more wave-number modes.

Recently, in elastic-wave turbulence, the analytical expression of the energy transfer has been reported in Ref. [4]. The elastic-wave turbulence has been used for numerical or experimental verification of the weak turbulence theory [5, 6]. In fact, the weak turbulence theory is valid in the large wave numbers where the nonlinearity is weak [5]. The strong turbulence also appears in the small wave numbers, and the weak turbulence and the strong turbulence coexist [7, 8]. The analytical expression of the energy transfer in Ref. [4] requires no assumptions about the nonlinearity, and hence it is exact and can be applied to the strong turbulence as well as the weak turbulence.

Such coexistence reminds us of an important conjecture for the energy transfer, i.e., critical balance in anisotropic turbulence [9]. The critical balance also in isotropic turbulence such as gravity water waves and Kelvin waves was suggested [10]. The critical balance predicts that the energy fluxes in the weak and strong turbulence are much different. However, the energy fluxes in the weak and strong turbulence in the elastic-wave turbulence are not much different because of the system's isotropy [4, 11]. The mechanism of the energy transfer in the coexistence of the weak and strong turbulence in the isotropic systems is needed to be understood carefully and quantitatively.

In the wave turbulence, large-amplitude structures localized in space and time are often found when the nonlinearity is large. An important example of the intermittent structures is the rogue wave, which is formed in oceans, optics, superfluid Helium, plasmas and so on. (See Ref. [12] and references therein.) The rogue wave is considered to be formed by the side-band instability of

* yokoyama@kuaero.kyoto-u.ac.jp

† mtakaoka@mail.doshisha.ac.jp

the energy-containing modes [13]. The relation between such intermittent structures and energy transfer has been claimed, though direct evidence has not been found yet. One of the difficulties in finding the evidence comes from the strong nonlinearity, which requires the evaluation of the energy transfer by including the nonlinear part of the energy in wave turbulence.

Such large-amplitude structures are also of interest in the mechanics of elastic membrane. When thin elastic sheets are deformed largely, the focusing of excessive strain leads to almost singular structures in the static crumpling of elastic membrane, such as developable cones (d -cones) and ridges. (See Ref. [14] and references therein.) The existence of dynamical crumpling, named after the analogy with the above static crumpling, are reported in Ref. [15] by simulating the unsteady elastic-wave turbulence. Although the dynamical crumpling does not reach the singular structures, the localized structures are remarkable for the strong nonlinearity. These large-scale structures exist in the strong turbulence, and they should give the mechanism of the energy transfer different from the resonant interactions in the weak turbulence. It is also observed in the elastic-wave turbulence that the non-Gaussian statistics of the fluctuation exhibits small-scale intermittency [16].

In this paper, the energy transfers in the elastic-wave turbulence are numerically investigated. The energy transfers between kinetic energy of a wave-number mode to stretching energy of another mode are quantitatively evaluated according to the triad interaction functions defined in Ref. [4]. The energy transfers in the small wave numbers are classified based on the system's nonlinearity, and then the transfers due to the large-scale structures are found to be much different from those due to the resonant interactions. We also investigate the energy transfer in the real space and the relation between the dynamics of the real-space structures and the energy transfer in the Fourier space. The transfers reveal the different mechanism of the nonlinear interactions in the weak and strong turbulence.

II. GOVERNING EQUATION AND NUMERICAL SIMULATIONS

The governing equation of elastic waves propagating in a thin plate is the Föppl-von Kármán (FvK) equation. The FvK equation is given as an equation for the displacement ζ [17, 18] as follows.

$$\rho \frac{\partial^2 \zeta}{\partial t^2} = -\frac{Yh^2}{12(1-\sigma^2)} \Delta^2 \zeta + \{\zeta, \chi\}, \quad (1)$$

where the auxiliary variable χ is the Airy stress potential defined as

$$\Delta^2 \chi = -\frac{Y}{2} \{\zeta, \zeta\}. \quad (2)$$

Here, Δ represents the Laplace operator, and

$$\{f, g\} = \frac{\partial^2 f}{\partial x^2} \frac{\partial^2 g}{\partial y^2} + \frac{\partial^2 f}{\partial y^2} \frac{\partial^2 g}{\partial x^2} - 2 \frac{\partial^2 f}{\partial x \partial y} \frac{\partial^2 g}{\partial x \partial y} \quad (3)$$

is the Monge–Ampère operator. The density ρ , the Young's modulus Y and the Poisson ratio σ are the material quantities of an elastic plate, and h denotes the thickness of the plate.

The momentum p is defined as

$$p = \rho \frac{\partial \zeta}{\partial t}. \quad (4)$$

Then, under the periodic boundary condition, the FvK equation (1), (2) and (4) is rewritten as

$$\frac{d\zeta_{\mathbf{k}}}{dt} = \frac{p_{\mathbf{k}}}{\rho}, \quad \frac{dp_{\mathbf{k}}}{dt} = -\rho \omega_{\mathbf{k}}^2 \zeta_{\mathbf{k}} + \sum_{\mathbf{k}_1 + \mathbf{k}_2 = \mathbf{k}} |\mathbf{k}_1 \times \mathbf{k}_2|^2 \zeta_{\mathbf{k}_1} \chi_{\mathbf{k}_2}, \quad (5a)$$

$$\chi_{\mathbf{k}} = -\frac{Y}{2k^4} \sum_{\mathbf{k}_1 + \mathbf{k}_2 = \mathbf{k}} |\mathbf{k}_1 \times \mathbf{k}_2|^2 \zeta_{\mathbf{k}_1} \zeta_{\mathbf{k}_2}, \quad (5b)$$

where $\zeta_{\mathbf{k}}$, $p_{\mathbf{k}}$ and $\chi_{\mathbf{k}}$ are the Fourier coefficients of the displacement, of the momentum, and of the Airy stress potential, respectively. The linear dispersion relation gives the frequency $\omega_{\mathbf{k}}$ as

$$\omega_{\mathbf{k}} = \sqrt{\frac{Yh^2}{12(1-\sigma^2)\rho}} k^2. \quad (6)$$

By introducing the complex amplitude defined as

$$a_{\mathbf{k}} = \frac{\rho \omega_{\mathbf{k}} \zeta_{\mathbf{k}} + i p_{\mathbf{k}}}{\sqrt{2\rho \omega_{\mathbf{k}}}}, \quad (7)$$

Eq. (5) is rewritten as

$$\begin{aligned} \frac{da_{\mathbf{k}}}{dt} = & -i\omega_{\mathbf{k}} a_{\mathbf{k}} \\ & - \frac{iY}{8\rho^2} \sum_{\mathbf{k}_1 + \mathbf{k}_2 + \mathbf{k}_3 = \mathbf{k}} \frac{|\mathbf{k} \times \mathbf{k}_1|^2 |\mathbf{k}_2 \times \mathbf{k}_3|^2}{|\mathbf{k}_2 + \mathbf{k}_3|^4} \\ & \times \frac{(a_{\mathbf{k}_1} + a_{-\mathbf{k}_1}^*)(a_{\mathbf{k}_2} + a_{-\mathbf{k}_2}^*)(a_{\mathbf{k}_3} + a_{-\mathbf{k}_3}^*)}{\sqrt{\omega_{\mathbf{k}} \omega_{\mathbf{k}_1} \omega_{\mathbf{k}_2} \omega_{\mathbf{k}_3}}}. \end{aligned} \quad (8)$$

Direct numerical simulation is performed according to the following equation, where the external force $F_{\mathbf{k}}$ and the dissipation $D_{\mathbf{k}}$ are added to make statistically-steady non-equilibrium states:

$$\frac{da_{\mathbf{k}}}{dt} = -i\omega_{\mathbf{k}} a_{\mathbf{k}} + \mathcal{N}_{\mathbf{k}} + F_{\mathbf{k}} + D_{\mathbf{k}}. \quad (9)$$

Here, $\mathcal{N}_{\mathbf{k}}$ represents the second term in the right-hand side of Eq. (8), which shows the four-wave nonlinear interactions. The external force $F_{\mathbf{k}}$ are artificially added to the small wave numbers so that $|a_{\mathbf{k}}|$ at $|\mathbf{k}| \leq 8\pi$ is constant in time. The dissipation is added as $D_{\mathbf{k}} =$

$-\nu|\mathbf{k}|^8 a_{\mathbf{k}}$, which is effective in the wave-number range $|\mathbf{k}| \gtrsim 256\pi$ in the present work.

The direct numerical simulation according to Eq. (9) is performed for a plate having the periodic boundary of $1\text{m} \times 1\text{m}$ according to Ref. [6], and then the two-dimensional wave-number vector \mathbf{k} is discretized as $\mathbf{k} \in (2\pi\mathbb{Z})^2$. The pseudo-spectral method, where the number of the aliasing-free modes is 512×512 , is employed. Details of the numerical scheme are explained in Ref. [7].

As a result of the numerical simulation, the energy spectrum shows the coexistence of the weak turbulence and the strong turbulence [4, 7, 8]. The weakly nonlinear spectrum which is a stationary solution of the kinetic equation [5], is observed in the large wave numbers. Another power law is observed in the small wave numbers, where the nonlinearity is relatively strong. The separation wave number of the weak and strong turbulence is located approximately at $k \approx 300$, which will be found in the energy spectra and the energy transfers in Fig. 6 below. We will investigate the energy transfers in this coexistence.

III. FORMULATION OF ENERGY TRANSFERS

A. Energy transfers in Fourier space

In this subsection, the energy transfers in the Fourier space is reviewed mostly following to Ref. [4]. The total energy of a wave-number mode $E_{\mathbf{k}}$ is given as the sum of the kinetic energy $K_{\mathbf{k}}$, the bending energy $V_{B\mathbf{k}}$ and the stretching energy $V_{S\mathbf{k}}$, i.e., $E_{\mathbf{k}} = K_{\mathbf{k}} + V_{B\mathbf{k}} + V_{S\mathbf{k}}$. Here,

$$K_{\mathbf{k}} = \frac{1}{2\rho}|p_{\mathbf{k}}|^2, \quad V_{B\mathbf{k}} = \frac{\rho\omega_{\mathbf{k}}^2}{2}|\zeta_{\mathbf{k}}|^2, \quad V_{S\mathbf{k}} = \frac{k^4}{2Y}|\chi_{\mathbf{k}}|^2. \quad (10)$$

These energies give the Hamiltonian of the FvK equation (5):

$$\mathcal{H} = \sum_{\mathbf{k}} \left(\frac{1}{2\rho}|p_{\mathbf{k}}|^2 + \frac{\rho\omega_{\mathbf{k}}^2}{2}|\zeta_{\mathbf{k}}|^2 + \frac{k^4}{2Y}|\chi_{\mathbf{k}}|^2 \right). \quad (11)$$

It must be noted that the representation of the nonlinear part of the Hamiltonian using the Airy stress potential $\chi_{\mathbf{k}}$ is not a mathematical trick. Originally, the stretching energy is given by the strain, and hence the Airy potential, which can be expressed by the displacement. Thus, the notation by the Airy stress potential is more primitive than that by the convolution of the displacement, and is in accordance with the derivation.

The energy transfer for each of decomposed energy can be derived by taking the time-derivatives of Eq. (10) and

substituting Eq. (5) into them (see also Ref. [4]):

$$T_{K\mathbf{k}} = \frac{\hat{d}K_{\mathbf{k}}}{\hat{d}t} = T_{K\mathbf{k}}^{(2)} + T_{K\mathbf{k}}^{(4)}, \quad (12a)$$

$$T_{K\mathbf{k}}^{(2)} = -\frac{\omega_{\mathbf{k}}^2}{2}p_{\mathbf{k}}^*\zeta_{\mathbf{k}} + \text{c.c.}, \quad (12b)$$

$$T_{K\mathbf{k}}^{(4)} = \frac{p_{\mathbf{k}}^*}{2\rho} \sum_{\mathbf{k}_1+\mathbf{k}_2=\mathbf{k}} |\mathbf{k}_1 \times \mathbf{k}_2|^2 \zeta_{\mathbf{k}_1} \chi_{\mathbf{k}_2} + \text{c.c.}, \quad (12c)$$

$$T_{B\mathbf{k}} = \frac{\hat{d}V_{B\mathbf{k}}}{\hat{d}t} = \frac{\omega_{\mathbf{k}}^2}{2}p_{\mathbf{k}}^*\zeta_{\mathbf{k}} + \text{c.c.}, \quad (12d)$$

$$T_{S\mathbf{k}} = \frac{\hat{d}V_{S\mathbf{k}}}{\hat{d}t} = -\frac{\chi_{\mathbf{k}}^*}{2\rho} \sum_{\mathbf{k}_1+\mathbf{k}_2=\mathbf{k}} |\mathbf{k}_1 \times \mathbf{k}_2|^2 p_{\mathbf{k}_1} \zeta_{\mathbf{k}_2} + \text{c.c.}, \quad (12e)$$

where $\hat{d}/\hat{d}t$ denotes the time-derivative in Eq. (5), and the external force and the dissipation are disregarded here. Note that Eq. (12) is obtained directly from Eq. (5) and Eq. (10) without any approximations. Then, the total-energy transfer is composed of these transfers as $T_{\mathbf{k}} = T_{K\mathbf{k}} + T_{B\mathbf{k}} + T_{S\mathbf{k}}$.

The cancellation of the quadratic part of the kinetic-energy transfer $T_{K\mathbf{k}}^{(2)}$ given as Eq. (12b) and the bending-energy transfer $T_{B\mathbf{k}}$ given as Eq. (12d), $T_{K\mathbf{k}}^{(2)} + T_{B\mathbf{k}} = 0$, corresponds to exchange between the kinetic and potential energies of the identical wave number as in the linear harmonic wave. Note that the exchange between the kinetic and bending energies in a wave number is referred to as transmutation shortly, and the transmutation is distinguished from the nonlinear energy transfer among different wave numbers. The bending energy increases or decreases only through this linear transmutation.

The quartic part of the kinetic-energy transfer $T_{K\mathbf{k}}^{(4)}$ and the stretching-energy transfer $T_{S\mathbf{k}}$ are the energy transfers due to the nonlinear interactions among triads $-\mathbf{k} + \mathbf{k}_1 + \mathbf{k}_2 = \mathbf{0}$.

By introducing the triad interaction functions,

$$T_{K\mathbf{k}\mathbf{k}_1\mathbf{k}_2}^{(4)} = \frac{|\mathbf{k}_1 \times \mathbf{k}_2|^2}{2\rho} p_{\mathbf{k}} \zeta_{\mathbf{k}_1} \chi_{\mathbf{k}_2} \delta_{\mathbf{k}+\mathbf{k}_1+\mathbf{k}_2, \mathbf{0}} + \text{c.c.}, \quad (13a)$$

$$T_{S\mathbf{k}\mathbf{k}_1\mathbf{k}_2} = -\frac{|\mathbf{k}_1 \times \mathbf{k}_2|^2}{2\rho} \chi_{\mathbf{k}} p_{\mathbf{k}_1} \zeta_{\mathbf{k}_2} \delta_{\mathbf{k}+\mathbf{k}_1+\mathbf{k}_2, \mathbf{0}} + \text{c.c.}, \quad (13b)$$

the nonlinear energy transfers can be written as

$$T_{K\mathbf{k}}^{(4)} = \sum_{\mathbf{k}_1, \mathbf{k}_2} T_{K\mathbf{k}\mathbf{k}_1\mathbf{k}_2}^{(4)}, \quad T_{S\mathbf{k}} = \sum_{\mathbf{k}_1, \mathbf{k}_2} T_{S\mathbf{k}\mathbf{k}_1\mathbf{k}_2}. \quad (14)$$

It should be noted here that the modes for \mathbf{k}_1 and \mathbf{k}_2 appearing in the triad interaction function of the total energy, $T_{\mathbf{k}\mathbf{k}_1\mathbf{k}_2}$, correspond to the different kinds of energies, while those for the Navier–Stokes equation are identical. For these triad interaction functions, a detailed energy

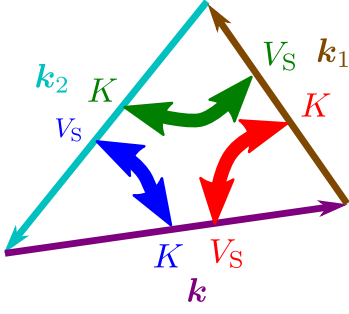


FIG. 1. (Color online) Detailed energy balance due to triad interactions: $T_{\mathbf{k}\mathbf{k}_1\mathbf{k}_2} + T_{\mathbf{k}_1\mathbf{k}_2\mathbf{k}} + T_{\mathbf{k}_2\mathbf{k}\mathbf{k}_1} = 0$.

balance can be derived

$$\begin{aligned}
& T_{\mathbf{K}\mathbf{k}\mathbf{k}_1\mathbf{k}_2}^{(4)} + T_{\mathbf{S}\mathbf{k}_2\mathbf{k}\mathbf{k}_1} \\
&= \frac{|\mathbf{k}_1 \times \mathbf{k}_2|^2}{2\rho} p \zeta_{\mathbf{k}_1} \chi_{\mathbf{k}_2} \delta_{\mathbf{k}+\mathbf{k}_1+\mathbf{k}_2, \mathbf{0}} + \text{c.c.} \\
&\quad - \frac{|\mathbf{k} \times \mathbf{k}_1|^2}{2\rho} \chi_{\mathbf{k}_2} p \zeta_{\mathbf{k}_1} \delta_{\mathbf{k}+\mathbf{k}_1+\mathbf{k}_2, \mathbf{0}} + \text{c.c.} \\
&= 0.
\end{aligned} \tag{15}$$

Different from the transmutation of the quadratic part, Eq. (15) represents that the stretching energy of \mathbf{k}_2 is transformed into the kinetic energy of \mathbf{k} and vice versa through the triad interaction $\mathbf{k} + \mathbf{k}_1 + \mathbf{k}_2 = \mathbf{0}$. It is of interest that the mode $\zeta_{\mathbf{k}_1}$ in $T_{\mathbf{K}\mathbf{k}\mathbf{k}_1\mathbf{k}_2}^{(4)}$ and the mode $\zeta_{\mathbf{k}_1}$ in $T_{\mathbf{S}\mathbf{k}_2\mathbf{k}\mathbf{k}_1}$ serves as a mediator between these two kinds of energies in the nonlinear interactions. This provides insight for gain or loss of the energies of the two wave-number modes in the triad in the elastic-wave turbulence, in marked contrast with the triad interaction in the Navier–Stokes turbulence.

The triad interaction function of the total energy, $T_{\mathbf{k}\mathbf{k}_1\mathbf{k}_2} = T_{\mathbf{K}\mathbf{k}\mathbf{k}_1\mathbf{k}_2}^{(4)} + T_{\mathbf{S}\mathbf{k}_2\mathbf{k}\mathbf{k}_1}$, satisfies the detailed energy balance through the triad interaction $\mathbf{k} + \mathbf{k}_1 + \mathbf{k}_2 = \mathbf{0}$:

$$T_{\mathbf{k}\mathbf{k}_1\mathbf{k}_2} + T_{\mathbf{k}_1\mathbf{k}_2\mathbf{k}} + T_{\mathbf{k}_2\mathbf{k}\mathbf{k}_1} = 0. \tag{16}$$

Namely, the triad interaction function shows the interchanges of the energy among the wave-number modes keeping the sum of the energies of the three wave-number modes.

The two kinds of the detailed energy balance, Eqs. (15) and (16), indicate that the energy is transferred by changing its form between the kinetic energy and the stretching energy owing to the triad interaction. The energy budget in the triad is schematically drawn in Fig. 1. It must be emphasized here again that though three wave-number modes appear in the triad interactions, we can identify from which mode or to which mode the energy is transferred in the elastic-wave turbulence. In other turbulent systems, the energy transfer of a wave-number mode is obtained only as the sum of the exchange with the multiple wave-number modes: with two wave-number modes in a triad interaction and with three modes in a quartet

interactions. Therefore, strong assumptions are usually required to identify the wave number from or to which mode the energy is transferred. For example, the locality of the nonlinear interactions was assumed in Ref. [19]. Since the combination of $\zeta_{\mathbf{k}_1}$ and $\chi_{\mathbf{k}_2}$ and that of $p_{\mathbf{k}_1}$ and $\zeta_{\mathbf{k}_2}$ are used as elementary modes in the triad interaction functions (13), and each mode corresponds to each wave number composing the triangle, we can clearly distinguish between the roles of \mathbf{k}_1 and \mathbf{k}_2 . It is highly advantageous to the identification of the details of the energy transfer.

B. Energy transfers in real space

In order to investigate the relation between the dynamics in the real space and the energy transfers in the Fourier space, we here define the energy transfers in the real space. At each location in the real space, the densities of the kinetic, bending and stretching energies are given as

$$K(\mathbf{x}) = \frac{1}{2\rho} p^2, \tag{17a}$$

$$V_B(\mathbf{x}) = \frac{Yh^2}{24(1-\sigma^2)} [(\Delta\zeta)^2 - (1-\sigma)\{\zeta, \zeta\}], \tag{17b}$$

$$V_S(\mathbf{x}) = \frac{1}{2Y} [(\Delta\chi)^2 - (1+\sigma)\{\chi, \chi\}]. \tag{17c}$$

The bending energy derives from the out-of-plane displacement, while the stretching energy comes from the in-plane strain. See, for example, Ref. [18].

Corresponding to Eq. (12), the decomposed energy transfers in the real space are defined here as follows:

$$\begin{aligned}
\frac{\partial K}{\partial t} &= T_K^{(2)}(\mathbf{x}) + T_K^{(4)}(\mathbf{x}) \\
&= -\frac{Yh^2}{12(1-\sigma^2)\rho} p \Delta^2 \zeta + \frac{1}{\rho} p \{\zeta, \chi\},
\end{aligned} \tag{18a}$$

$$\begin{aligned}
\frac{\partial V_B}{\partial t} &= T_B^{(2)}(\mathbf{x}) + T_B^{(D)}(\mathbf{x}) \\
&= \frac{Yh^2}{12(1-\sigma^2)\rho} (\Delta\zeta)(\Delta p) - \frac{Yh^2}{12(1+\sigma)\rho} \{\zeta, p\},
\end{aligned} \tag{18b}$$

$$\begin{aligned}
\frac{\partial V_S}{\partial t} &= T_S^{(4)}(\mathbf{x}) + T_S^{(D)}(\mathbf{x}) \\
&= -\frac{1}{\rho} (\Delta\chi)(\Delta^{-1}\{\zeta, p\}) + \frac{1+\sigma}{\rho} \{\chi, \Delta^{-2}\{\zeta, p\}\}.
\end{aligned} \tag{18c}$$

Note that both $T_B^{(D)}(\mathbf{x})$ and $T_S^{(D)}(\mathbf{x})$ have divergence forms, because the Monge–Ampère operator can be

rewritten as

$$\{f, g\} = \frac{\partial}{\partial x} \left(\frac{\partial f}{\partial x} \frac{\partial^2 g}{\partial y^2} - \frac{\partial f}{\partial y} \frac{\partial^2 g}{\partial x \partial y} \right) + \frac{\partial}{\partial y} \left(\frac{\partial f}{\partial y} \frac{\partial^2 g}{\partial x^2} - \frac{\partial f}{\partial x} \frac{\partial^2 g}{\partial x \partial y} \right). \quad (19)$$

The representation that is more similar to Eq. (12) can be obtained by integrating these expressions over a finite area A and by using partial integral:

$$\begin{aligned} \frac{\partial \mathcal{K}}{\partial t} &= T_{\mathcal{K}}^{(2)} + T_{\mathcal{K}}^{(4)} \\ &= -\frac{Yh^2}{12(1-\sigma^2)\rho} \int_A p \Delta^2 \zeta dA + \frac{1}{\rho} \int_A p \{\zeta, \chi\} dA, \\ \frac{\partial \mathcal{V}_B}{\partial t} &= T_B^{(2)} + T_B^{(D)} \\ &= \frac{Yh^2}{12(1-\sigma^2)\rho} \int_A p \Delta^2 \zeta dA + \text{B.V.}(\partial A), \\ \frac{\partial \mathcal{V}_S}{\partial t} &= T_S^{(4)} + T_S^{(D)} \\ &= -\frac{1}{\rho} \int_A \chi \{p, \zeta\} dA + \text{B.V.}(\partial A), \end{aligned} \quad (20)$$

where $\text{B.V.}(\partial A)$ stands for the boundary values surrounding the finite area A . These expressions more clearly show the energy balance among the kinetic, bending, and stretching energies than those in Eq. (18). For example, a similar expression corresponding to the detailed energy balance, Eq. (15), can be written as

$$\begin{aligned} T_{\mathcal{K}}^{(4)} + T_S^{(4)} &= \frac{1}{\rho} \int_A p \{\zeta, \chi\} dA - \frac{1}{\rho} \int_A \chi \{p, \zeta\} dA \\ &= \text{B.V.}(\partial A). \end{aligned} \quad (22)$$

When the area A is the whole domain, we obtain $\text{B.V.}(\partial A) = 0$ owing to the periodic boundary condition.

IV. RESULTS

A. Detailed energy transfers among wave-number modes

To investigate the detailed energy balance through the triad interaction functions (see Eq. (15)), the azimuthally-integrated energy transfer functions are de-

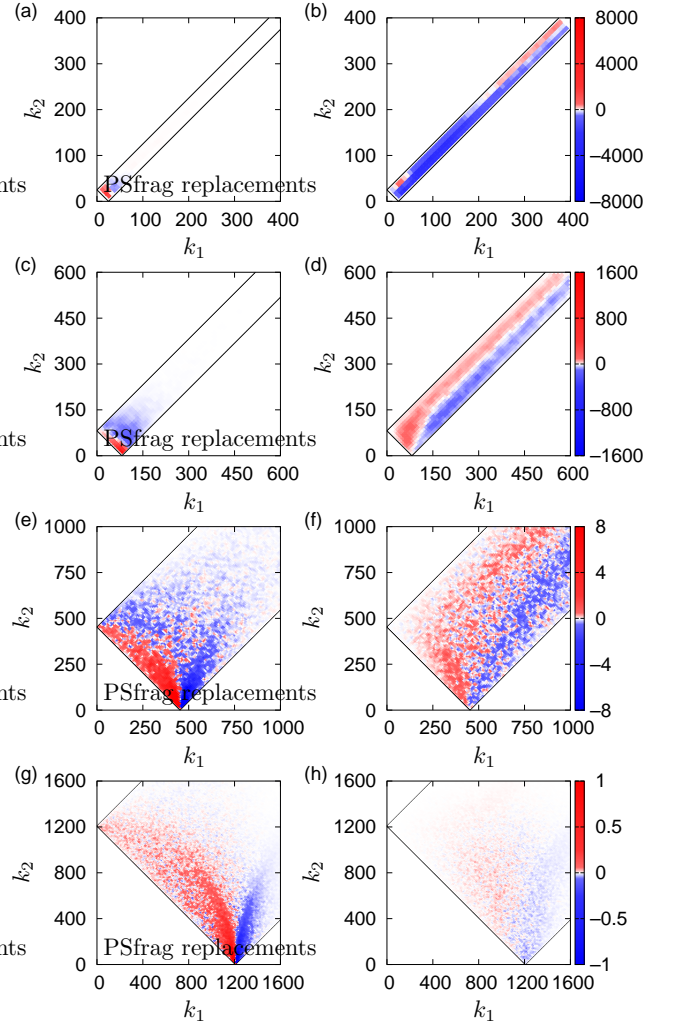


FIG. 2. (Color) Energy transfer functions. (a) and (b): to $|\mathbf{k}| = 8\pi$, (c) and (d): to $|\mathbf{k}| = 26\pi$, (e) and (f): to $|\mathbf{k}| = 144\pi$, and (g) and (h): to $|\mathbf{k}| = 384\pi$. (a), (c), (e) and (g): to kinetic energy $\mathcal{T}_{\mathbf{k}\mathbf{k}}^{(4)}(k_1, k_2)$, where k_1 and k_2 are respectively the wave numbers for ζ and χ as defined in Eq. (23a), and (b), (d), (f) and (h): to stretching energy $\mathcal{T}_{S\mathbf{k}}(k_1, k_2)$, where k_1 and k_2 are respectively the wave numbers for p and ζ as defined in Eq. (23b).

defined as

$$\begin{aligned}\mathcal{T}_{K\mathbf{k}}^{(4)}(k_1, k_2) &= \frac{1}{\Delta k_1 \Delta k_2} \sum'_{\mathbf{k}'_1, \mathbf{k}'_2} T_{K\mathbf{k}\mathbf{k}'_1\mathbf{k}'_2}^{(4)} \\ &= \frac{1}{\Delta k_1 \Delta k_2} \sum'_{\mathbf{k}'_1, \mathbf{k}'_2} \frac{|\mathbf{k}'_1 \times \mathbf{k}'_2|^2}{2\rho} p_{\mathbf{k}} \zeta_{\mathbf{k}'_1} \chi_{\mathbf{k}'_2} \delta_{\mathbf{k}+\mathbf{k}'_1+\mathbf{k}'_2, \mathbf{0}} + \text{c.c.},\end{aligned}\quad (23a)$$

$$\begin{aligned}\mathcal{T}_{S\mathbf{k}}(k_1, k_2) &= \frac{1}{\Delta k_1 \Delta k_2} \sum'_{\mathbf{k}'_1, \mathbf{k}'_2} T_{S\mathbf{k}\mathbf{k}'_1\mathbf{k}'_2} \\ &= -\frac{1}{\Delta k_1 \Delta k_2} \sum'_{\mathbf{k}'_1, \mathbf{k}'_2} \frac{|\mathbf{k}'_1 \times \mathbf{k}'_2|^2}{2\rho} \chi_{\mathbf{k}} p_{\mathbf{k}'_1} \zeta_{\mathbf{k}'_2} \delta_{\mathbf{k}+\mathbf{k}'_1+\mathbf{k}'_2, \mathbf{0}} + \text{c.c.},\end{aligned}\quad (23b)$$

where $\sum'_{\mathbf{k}'_1, \mathbf{k}'_2}$ denotes the summation over $|\mathbf{k}'_1 - \mathbf{k}_1| < \Delta k_1/2$ and $|\mathbf{k}'_2 - \mathbf{k}_2| < \Delta k_2/2$. Here, $\Delta k_1 = \Delta k_2 = 2\pi$ is employed. The energy transfer functions shown in the following figures 2 and 3 are obtained by averaging over 1024 realizations, 4 different times, and directions of \mathbf{k} . The time interval of the 4 different times is sufficiently longer than the longest linear period to validate the statistical independence. The numbers of the samples averaged over the directions \mathbf{k} are at least 6, which is for $k = 8\pi$. We compared the result with those obtained by reduced numbers of the samples and by different Δk_1 and Δk_2 , and the result is confirmed to be robust.

These energy transfer functions are drawn in Fig. 2 for four representative wave numbers. The wave number $|\mathbf{k}| = 8\pi \approx 25$ is in the forcing range. Both of the wave numbers $26\pi \approx 82$ and $144\pi \approx 450$ are in the inertial subrange; the former is in the strong turbulence range, and the latter in the weak turbulence range. The wave number $384\pi \approx 1200$ is in the dissipation range. Note that the area is restricted within a diagonal rectangle corresponding to the triangle inequality, i.e., $|\mathbf{k}_1 - \mathbf{k}_2| < k < k_1 + k_2$. The magnitude of $|\mathbf{k}|$ corresponds to the corner of the diagonal rectangle.

For the wave numbers $|\mathbf{k}| = 8\pi$ (Fig. 2(a)), the kinetic-energy transfer is positive for the wave numbers smaller than itself. Namely, $K_{\mathbf{k}}$ obtains the energy from $V_{S\mathbf{k}_2}$ where $k_2 < k$. The stretching energy is distributed over broad wave numbers whose magnitude are $50 \lesssim k_1 \lesssim 200$. (Fig. 2(b)) It exhibits that the energy is transferred comparatively nonlocally to the wave numbers much larger than 8π . The sign of the stretching-energy transfer is always negative in $50 \lesssim k_1 \lesssim 200$. Thus, the nonlocal transfers are statistically significant.

As shown in Fig. 2(c), the wave numbers in the inertial subrange of the strong turbulence, $|\mathbf{k}| = 26\pi$, obtain the energy as its kinetic energy nonlocally from small k_2 . The energy transfer from $k_2 \approx 0$ is substantial because the sign of the energy transfer is always positive near the corner. It is consistent with the loss of the stretching energy of the wave numbers in the forcing range shown in Fig. 2(b). On the other hand, $V_{S\mathbf{k}}$ obtains the energy from k_1 when $k_1 < k$ or $k_1 < k_2$, while it gives the energy to $V_{S\mathbf{k}_1}$ when $k_1 > k, k_2$ (Fig. 2(d)).

The wave number in the inertial subrange of the weak turbulence, $|\mathbf{k}| = 144\pi$, has both positive and negative values of the kinetic-energy transfer near the bottom corner where $k_2 \ll k$ (Fig. 2(e)). It is in contrast with the positive values near the corner for the wave numbers in the forcing range and strong turbulence (Figs. 2(a) and (c)). The energy transfers are consistent with the negative and positive values at $k_1 = 144\pi \approx 450$ in Figs. 2(b) and (d). The energy transfer function of the stretching energy at $|\mathbf{k}| = 144\pi$ (Fig. 2(f)) is similar with that at $|\mathbf{k}| = 26\pi$ (Fig. 2(d)) because the self-similar cascading transfer is dominant. This self-similarity makes similar structures in the energy transfer functions at $|\mathbf{k}| = 384\pi$ in the dissipation range. (Figs. 2(g) and (h))

According to Eqs. (13) and (15), the energy is transferred between the kinetic energy of a wave-number mode and the stretching energy of another wave-number mode owing to the nonlinear interactions. The wave number of ζ which consists of a triad mediates the energy transfers between the kinetic energy and stretching energy without changing its bending energy by the nonlinear interactions. Thus, the wave number of ζ does not contribute directly to the redistribution of energy among the modes. By virtue of this remarkable nature of the nonlinear interactions in the elastic-wave turbulence, integration over the wave numbers of ζ clarifies the energy transfer between the kinetic energy of a wave number and the stretching energy of another wave number. We here refer to the energy transfer functions integrated over the wave numbers of ζ as binary energy transfers. The binary energy transfer $\mathcal{T}_{K\mathbf{k}}^{(4)}$ to the kinetic energy of \mathbf{k} from the stretching energy of k_2 and $\mathcal{T}_{S\mathbf{k}}$ to the stretching energy of \mathbf{k} from the kinetic energy of k_1 are, respectively, defined as

$$\mathcal{T}_{K\mathbf{k}}^{(4)}(k_2) = \int \mathcal{T}_{K\mathbf{k}}^{(4)}(k_1, k_2) dk_1 = \frac{1}{\Delta k_2} \sum'_{\mathbf{k}'_2} \sum'_{\mathbf{k}'_1} T_{K\mathbf{k}\mathbf{k}'_1\mathbf{k}'_2}^{(4)},\quad (24a)$$

$$\mathcal{T}_{S\mathbf{k}}(k_1) = \int \mathcal{T}_{S\mathbf{k}}(k_1, k_2) dk_2 = \frac{1}{\Delta k_1} \sum'_{\mathbf{k}'_1} \sum'_{\mathbf{k}'_2} T_{S\mathbf{k}\mathbf{k}'_1\mathbf{k}'_2},\quad (24b)$$

where $\sum'_{\mathbf{k}'_1}$ and $\sum'_{\mathbf{k}'_2}$ respectively denote the summations over $|\mathbf{k}'_1 - \mathbf{k}_1| < \Delta k_1/2$ and $|\mathbf{k}'_2 - \mathbf{k}_2| < \Delta k_2/2$.

The binary energy transfers to the four representative wave numbers are drawn in Fig. 3, where Δk_i is 2π for $k_i < 26\pi$ and logarithmically-scaled for $k_i \geq 26\pi$. In forcing range, $|\mathbf{k}| = 8\pi$ (Fig. 3(a)), the mode obtains the energy as the kinetic energy from the smaller wave numbers as known from the fact that the transfer of the kinetic energy $\mathcal{T}_{K\mathbf{k}}^{(4)}(k_1, k_2)$ is large for small k_2 . (Fig. 2(a)) Since the transfer of the stretching energy, $\mathcal{T}_{S\mathbf{k}}(k_1)$, is negatively large in the range $50 \lesssim k_1 \lesssim 200$, $V_{S\mathbf{k}}$ at this scale is transferred nonlocally to $K_{\mathbf{k}_1}$ in this range. The nonlocal interactions are not fluctuations but statistically significant as seen in Fig. 2(b).

In the inertial subrange of the strong turbulence, $|\mathbf{k}| =$

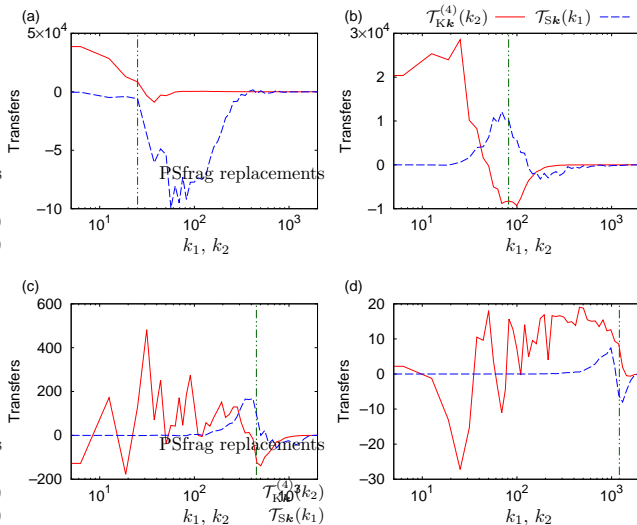


FIG. 3. (Color online) Binary energy transfer functions $\mathcal{T}_{Kk}^{(4)}(k_2)$ and $\mathcal{T}_{Sk}(k_1)$ from wave numbers k_1 or k_2 (a) to $|\mathbf{k}| = 8\pi$, (b) to $|\mathbf{k}| = 26\pi$, (c) to $|\mathbf{k}| = 144\pi$ and (d) to $|\mathbf{k}| = 384\pi$. The vertical lines show the representative wave numbers $|\mathbf{k}|$. The abscissa is scaled logarithmically.

26π (Fig. 3(b)), the wave number obtains the kinetic energy nonlocally from the wave numbers in the forcing range $k_2 \leq 8\pi$. It is consistent with the loss of $V_{S\mathbf{k}}$ in the forcing range as shown in Fig. 3(a). The fact that the energy transfers from the forcing range are comparable in Figs. 3(a) and (b) supports the large redistribution of the energy over broad wave numbers. The transfer from $K_{\mathbf{k}}$ to $V_{S\mathbf{k}_2}$ at k_2 slightly larger than 26π , is also noticeable. The stretching energy at this scale $V_{S\mathbf{k}}$ obtains the energy from $K_{\mathbf{k}_1}$ where k_1 is slightly smaller than 26π , and gives the energy to $K_{\mathbf{k}_1}$ where $150 \lesssim k_1 \lesssim 300$. These interactions between comparable-scale modes repeatedly transfer the kinetic and stretching energies from the smaller to larger wave numbers, and locally cascades energy step by step. Therefore, the nonlocal interactions with the wave-number modes in the forcing range and the local interactions between comparable-scale modes coexist in the strong turbulence. The stretching-energy transfer, $\mathcal{T}_{Sk}(k_1)$, for $k_1 \gtrsim 400$ is almost 0. It indicates that the positive and negative stretching-energy transfers in the large wave numbers $k_1, k_2 \gg k$ in Fig. 2(d) cancel each other. The cancellation indicates that such nonlocal interactions do not cause net energy transfer. It represents the “drift” of the small-scale wave \mathbf{k}_1 due to the large-scale wave of \mathbf{k} resulting mainly in the small change of the direction of the small-scale wave. It is similar with the sweeping effect known in the homogeneous isotropic Navier–Stokes turbulence [3]. It must be noted again that the nonlocal interactions between $K_{\mathbf{k}}$ where \mathbf{k} is in the strong turbulence range and $V_{S\mathbf{k}}$ where \mathbf{k} is in the forcing range cause the net energy transfer, and such statistically-significant nonlocal interactions are different from the sweeping effect.

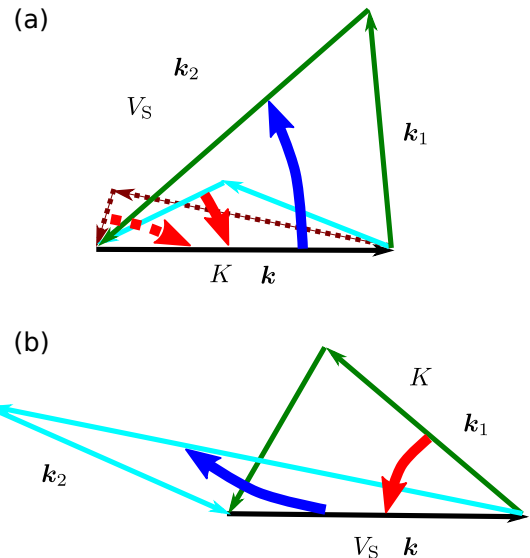


FIG. 4. (Color online) Schematic net energy transfers due to the local interactions (solid arrows) and that due to the nonlocal interactions (dotted arrows). (a) $\mathcal{T}_{Kk}^{(4)}$ and (b) $\mathcal{T}_{Sk}^{(4)}$.

The wave number in the inertial subrange of the weak turbulence $|\mathbf{k}| = 144\pi$ (Fig. 3(c)) and that in the dissipation range $|\mathbf{k}| = 384\pi$ (Fig. 3(d)) show the locally-cascading kinetic- and stretching-energy transfers in the same manner as the local interactions in the strong turbulence. The nonlocal interactions with the forced wave numbers for the kinetic-energy transfers much fluctuate, and are not statistically significant. The fluctuations are caused by the large positive and negative values near the corner $k_2 \approx 0$ in Figs. 2(e) and (g), and should be statistically canceled. The tendency of the cancellation was confirmed by comparison with the fluctuation in the fewer samples. It represents the drift of the small-scale wave \mathbf{k} due to the large-scale wave \mathbf{k}_2 , and it is the counterpart of the drift observed in large wave numbers in Fig. 3(b). Therefore, though we observe that the large energy transfers from the wave numbers in $k_1^2 + k_2^2 < k^2$ and $k_1 + k_2 > k$ in Figs. 2(e) and (g), only these local interactions between comparable-scale modes in the wave-number range contribute the net energy transfers. It should be noted here that the scale of the vertical axes of Figs. 3(c) and (d) is respectively smaller by two and three orders of magnitude than those of Figs. 3(a) and (b). Even if there exist similar fluctuations in Figs. 3(a) and (b), they cannot be observed there owing to the substantial energy transfers.

From Figs. 2 and 3, we can extract the shape of the triad interaction for the net energy transfers, which are schematically summarized in Fig. 4. The thick arrows represent the energies from or to the wave number \mathbf{k} . Through the triad interactions of $T_{\mathbf{k}k_1k_2} + T_{k_1k_2\mathbf{k}} + T_{k_2k\mathbf{k}_1} = 0$, $K_{\mathbf{k}}$ whose wave number \mathbf{k} is in the inertial subrange is transformed from or into $V_{S\mathbf{k}_2}$ (Fig. 4(a)),

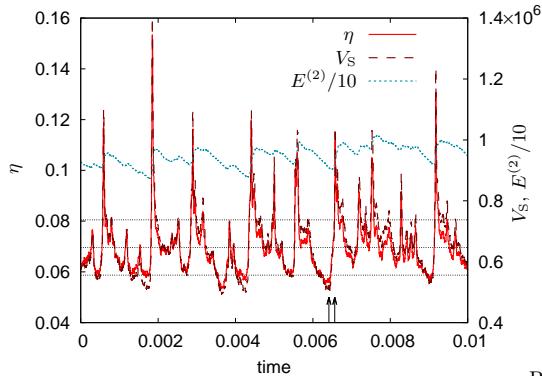


FIG. 5. (Color online) Times series of nonlinearity η (left axis), and linear energy $E^{(2)}$ and nonlinear energy V_S . The linear energy is divided by 10 for visibility. The mean of η and ± 1 -sigma levels are represented by dotted lines. Two arrows at bottom indicate the representative times: moderate phase and active phase.

while $V_{S\mathbf{k}}$ is transformed from or into $K_{\mathbf{k}_1}$ (Fig. 4(b)). Note that only representative triads are shown in this figure. In particular, the lengths of the wave numbers of ζ , \mathbf{k}_1 in Fig. 4(a) and \mathbf{k}_2 in Fig. 4(b), are comparatively variable, which indicates that the triangle can be obtuse-angled as well as acute-angled.

In Fig. 4(a), the wave number \mathbf{k} that is either in the weak turbulence and the strong turbulence obtains the kinetic energy from the stretching energy of \mathbf{k}_2 through the triad that is $k_1, k_2 \approx k/2$ and k_1 slightly larger than k_2 . (flattened triangle) On the other hand, $K_{\mathbf{k}}$ gives the energy to $V_{S\mathbf{k}_2}$ through the triad where k_2 is slightly larger than k . (nearly-equilateral triangle) As written above, the length of \mathbf{k}_1 is comparatively variable. These two transfers are caused by the local interactions in the Fourier space, and observed all over the wave numbers, The thick dotted arrow represents the nonlocal kinetic-energy transfer directly from the stretching energy of the small wave number \mathbf{k}_2 that is in the forcing range. The nonlocal transfer emerges only if the wave number \mathbf{k} is in the strong turbulence. (dotted triangle)

The stretching-energy transfer $T_{S\mathbf{k}\mathbf{k}_1\mathbf{k}_2}$ shown in Fig. 4(b) has only the local interactions. Corresponding to the kinetic-energy transfer, $V_{S\mathbf{k}}$ decreases by giving the energy to $K_{\mathbf{k}_1}$ where $k_1 \approx 2k$. (flattened triangle) In the same manner, $V_{S\mathbf{k}}$ increases by obtaining the energy as $K_{\mathbf{k}_1}$ whose k_1 slightly larger than k . (nearly-equilateral triangle) Similarly to the kinetic-energy transfer $T_{K\mathbf{k}\mathbf{k}_1\mathbf{k}_2}$, the locally-cascading energy transfers are observed all over the wave numbers.

B. Energy transfers in active and moderate phases

The typical time series of the nonlinearity as well as the linear and nonlinear energies are drawn in Fig. 5. The intermittency leads us to investigate the energy trans-

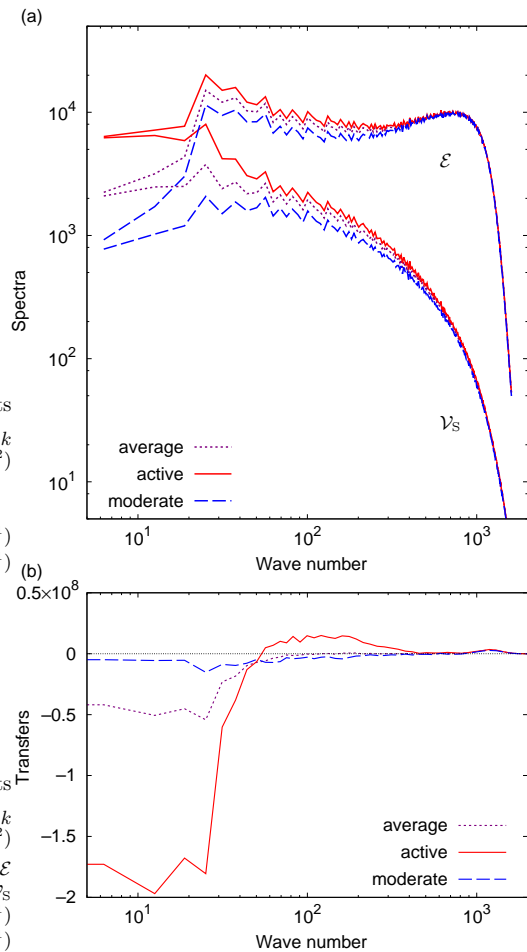


FIG. 6. (Color online) (a): Total-energy spectra \mathcal{E} and stretching-energy spectra \mathcal{V}_S , and (b): energy transfer for overall average and those for the active and moderate phases.

fer by dividing the phases of the system into active and moderate phases. The active and moderate phases are classified by the nonlinearity of the system.

The nonlinearity is defined as the ratio of the nonlinear energy to the linear energy: $\eta = V_S/E^{(2)} = \sum_{\mathbf{k}} V_{S\mathbf{k}} / \sum_{\mathbf{k}} (K_{\mathbf{k}} + V_{B\mathbf{k}})$. The nonlinear energy (dashed curve) shows strong temporal intermittency, which has sawtooth-wave profile with sudden jumps and slow relaxations, while the jumps of the linear energy (dotted curve) are synchronized, but are not so large. It results in resemblance between strong temporal intermittency of the nonlinear energy and the that of the nonlinearity (solid curve). In this work, the active phases when the system has strong nonlinearity are defined so that $\eta > \langle \eta \rangle + \sqrt{\langle (\eta - \langle \eta \rangle)^2 \rangle}$, while the moderate phases are the phases when $\eta < \langle \eta \rangle - \sqrt{\langle (\eta - \langle \eta \rangle)^2 \rangle}$. Here, $\langle \cdot \rangle$ represents averaging over ensembles, and 4096 fields are used as ensembles. As a result, the numbers of statistically-independent wave fields in the active phase and in the moderate phase are respectively 521 and 393.

The total-energy spectrum and the stretching-energy

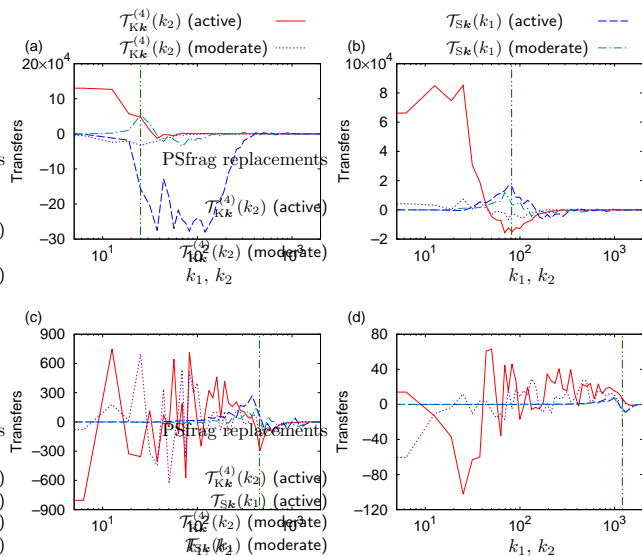


FIG. 7. (Color online) Binary energy transfers at active and moderate phases. See the figure caption of Fig. 3.

spectrum for the overall average and those for the active and moderate phases are drawn in Fig. 6(a). Obviously, the intermittency results mainly from the fluctuation of the stretching energy in the small and middle wave-number ranges ($k \gtrsim 400$), i.e., in forcing and strong turbulence ranges. No significant difference appears in the large wave numbers, i.e., in the weak turbulence range, which is consistent with the weak turbulence theory. On the other hand, the spectra of the kinetic and bending energies are not so different between the active and moderate phases, though they are not drawn here.

As examined in Ref. [4], one-dimensionalized energy transfers, $\mathcal{T}(k) = (\Delta k)^{-1} \sum_{|k'-k| < \Delta k/2} T_{k'}$, at the active and moderate phases are drawn in Fig. 6(b). The energy transfer at the active phases shows negatively large values for the wave-number modes in the forcing range and positive values for the wave-number modes in the strong turbulence range, while the energy transfer at the moderate phases is small negative in both of the wave-number ranges. At these active phases, the energy obtained from the external force in the forcing range as the stretching energy is distributed over the wave-number modes in the strong turbulence. The energy transfer is relaxed to the normal state at other phases.

To identify the energy balance between two wave-number modes at these phases, the binary energy transfers at the active phase and at the moderate phase at the four representative wave numbers are drawn in Fig. 7. (See also Fig. 3.) The remarkable difference between these phases is found at the wave number $|\mathbf{k}| = 8\pi$ in the forcing range (Fig. 7(a)) and the wave number $|\mathbf{k}| = 26\pi$ in the strong turbulence range (Fig. 7(b)). At the wave number $|\mathbf{k}| = 144\pi$ in the weak turbulence (Fig. 7(c)) only slight difference in finite range can be seen though it is hidden in the fluctuation: $\mathcal{T}_{S144\pi}$ in the

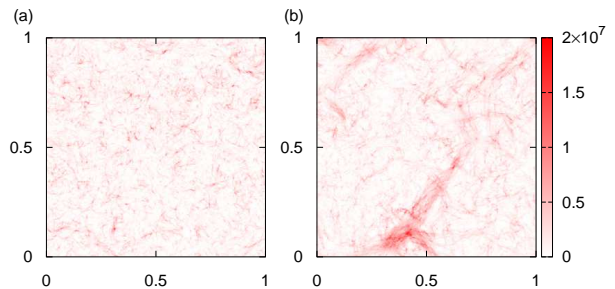


FIG. 8. (Color online) Real-space structures in stretching energy fields at moderate phase (a) and at active phase (b) pointed out by arrows in Fig. 5.

active phase is larger than that in the moderate phase in $200 \lesssim k_1 \lesssim 400$, and $\mathcal{T}_{K144\pi}$ in $100 \lesssim k_2 \lesssim 300$. No clear difference within the fluctuation error can be observed at the wave numbers $|\mathbf{k}| = 384\pi$ in the dissipation range (Fig. 7(d)).

The nonlocal energy transfer from $V_{S\mathbf{k}}$ where \mathbf{k} is in the forcing range ($\mathcal{T}_{S8\pi}(k_1)$ at the active phase in Fig. 7(a)) to $K_{\mathbf{k}}$ where \mathbf{k} is in the strong turbulence ($\mathcal{T}_{K26\pi}(k_2)$ at the active phase in Fig. 7(b)) emerges only at the active phase. It is clear that the stretching energy in the forcing range is distributed widely over the wave numbers in the strong turbulence through the nonlocal energy transfer. The local energy transfers between comparable-scale modes are observed both at the active phases and the moderate phases and at all the wave numbers. The nonlocal energy transfer plays a crucial role only at the active phase in the forcing range or in the strong turbulence. In other words, the local and nonlocal energy transfers coexist at the active phase, while only the local energy transfer is effective at the moderate phase.

Next, energy transfer at each phase is examined from the view point of real-space structures. Since we have observed that the stretching energy causes the intermittency, the stretching energy in the real space, which is defined as Eq. (17c), is drawn in Fig. 8. While the stretching-energy field at a moderate phase pointed out by the left arrow of a pair of arrows in Fig. 5 is drawn in Fig. 8(a), that at an active phase pointed out by the right arrow is drawn in Fig. 8(b) as representative. One can observe a distinctive structure lying in the center of lower half part in this figure. The distinctive structure is composed of two bundles of the fibrous structures, and is in the form of the laterally reversed image of the character λ . A point-like structure appears at the joint of the two bundles, i.e., roughly at (0.4, 0.1). The bundle structures and the point-like structures appear intermittently, and they are similarly observed in the field of the von Mises stress, which is used for a criterion of yielding. The slender elongated structures, i.e., the bundle structures, are expected to reflect the nonlocal interaction of the energy transfer at the active phases shown in Fig. 7(a), since the lengths and the widths of such structures are, respectively, $k \sim 2\pi \times O(1)$ and $k \sim 2\pi \times O(10)$. The nonlocal

property of energy transfer has been discussed also in the Navier–Stokes turbulence, where very thin and elongated intense vortices are responsible for anomalous corrections to the cascade theory. In two-dimensional Navier–Stokes turbulence, especially, reported are the nonlocality of the enstrophy cascade citing the coherent vortices and the importance of the nonlocal feedback of small scales on large scales, e.g., Ref. [20].

The point-like structures and the bundle structures might remind us of the d -cones and the ridges of the displacement ζ in the real space observed in laboratory experiments. Although the point-like structures and the bundle structures are distinct in the field of stretching energy, the d -cones and the ridges could not be observed clearly in the field of ζ in the present simulation. The point-like structures and the bundle structures show the concentration of the stress, and they would result in the d -cones and the ridges in much higher nonlinear state, because the relation between the structures in ζ and those in the energy dissipation field is reported in numerical simulations for strongly nonlinear field [15].

It should be noted that though there are no large-scale bundle structures, small unilaminar fibrous structures and resulting point structures can be observed even at the moderate phase (Fig. 8(a)), which might be related to recently-reported small-scale intermittency [16]. At both phases, small-scale fibrous structures are found also in the gradient field of displacement $|\nabla\zeta|$ [15], though the magnitude at the active phase is much larger than that at the moderate phase. These strongly-nonlinear structures that dynamically emerge are observed only in numerical experiments. The observation in laboratory experiments is expected.

The energy transfers at each location in the real space defined as Eqs. (18a) and (18c) are drawn in Fig. 9. As a representative of the moderate phase, Figs. 9(a) and (b) are drawn at the same time of Fig. 8(a). Similarly, Figs. 9(c) and (d) correspond to Fig. 8(b) in time. At the active phase, the energy transfers are large around the bundle of the fibrous structures near (0.5, 0.2), though it might be difficult to be recognized owing to the numerous small-scale variation.

To observe the energy transfer in the real space more clearly, the coarse-graining of the finite area A in §III B is employed for the fields in Fig. 10. The energy transfers which are coarse-grained with the scale r_{CG} at the active phase are drawn in Fig. 10. In Figs. 10(a) and (b), the coarse-grained transfers are averaged over the grid points \mathbf{x}' in $|\mathbf{x}' - \mathbf{x}| < r_{CG} = 1/4$. The scale corresponds to $k_{CG} = 8\pi$ in the forcing range. Similarly, the coarse-grained transfers with the scale $r_{CG} = 1/16$, and those with the scale $r_{CG} = 1/64$ are drawn in Figs. 10(c) and (d), and in Figs. 10(e) and (f), respectively. The scale $r_{CG} = 1/16$ and the scale $r_{CG} = 1/64$, respectively, correspond to the wave number $k_{CG} = 32\pi$ in the strong turbulence and to the wave number $k_{CG} = 128\pi$ in the weak turbulence.

In the coarse-grained transfers with the scale $r_{CG} =$

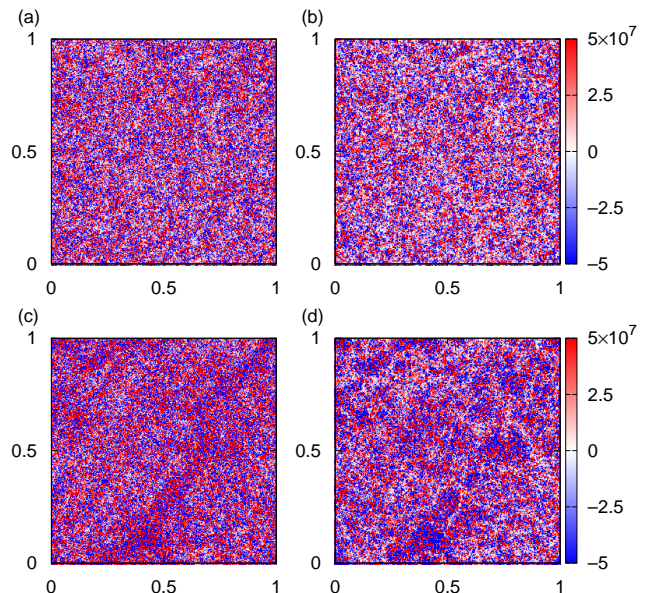


FIG. 9. (Color) Energy transfers in real space. (a) and (b): at moderate phase, and (c) and (d): at active phase. (a) and (c): to kinetic energy $T_K^{(4)}(\mathbf{x})$, and (b) and (d): to stretching energy $T_S(\mathbf{x})$.

$1/4$ (Figs. 10(a) and (b)), it is found that the bundle structures play a dominant role in the energy transfer; the scale gains the kinetic energy, and loses the stretching energy. The coarse-grained transfer of the kinetic energy with the scale $r_{CG} = 1/4$ is positive almost everywhere, while that of the stretching energy is negative. They are consistent with the energy transfers in the Fourier space as shown in Fig. 3(a).

In the coarse-grained transfers with the scale $r_{CG} = 1/16$ (Figs. 10(c) and (d)), the energy transfers in the vicinity of the bundle structures are a little less remarkable, and the positive and negative regions are mixed in confusion in the region away from the bundle structures. However, the kinetic-energy and stretching-energy transfers, respectively, tend to positive and negative near the bundle structure in this field. In fact, the kinetic-energy and stretching-energy transfers are positive and negative on average, respectively.

The coarse-grained transfers with the scale $r_{CG} = 1/64$ (Figs. 10(e) and (f)) are similar with those without coarse-graining as shown in Fig. 9. The large energy transfers in the bundle structures can be recognized with an effort.

At the moderate phase, the regions of the positive and negative transfers are mixed for any scales, though the figure is omitted here. Thus, no characteristic structures are found as anticipated from Fig. 8(a). Even in the largest scale $r_{CG} = 1/4$, both the negative and the positive regions of energy transfers appear in contrast with those at the active phase shown in Figs. 10(a) and (b). Although no distinctive structures can be observed in all the contours of Fig. 10, The negative correlations be-

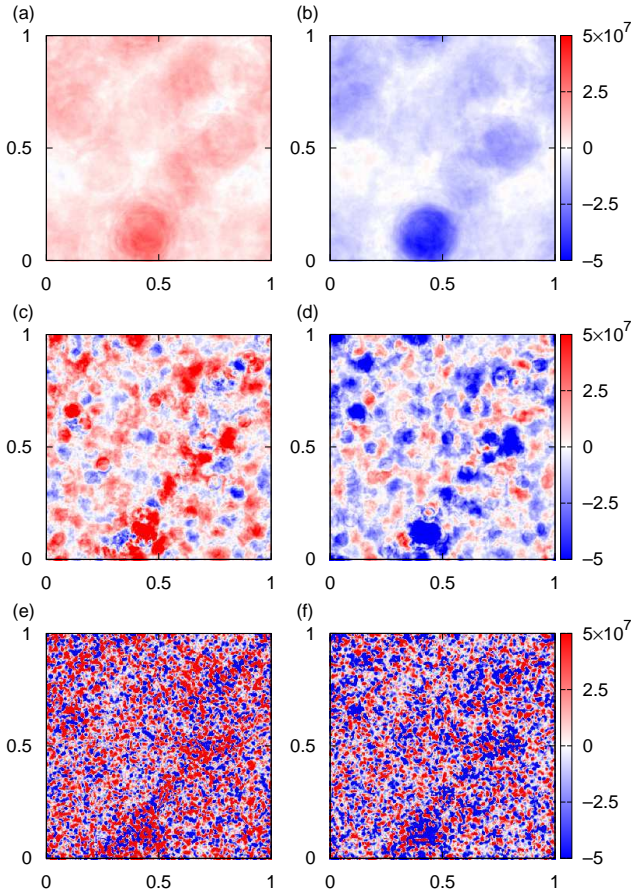


FIG. 10. (Color) Coarse-grained energy transfers in real space at active phase. (a) and (b): $r_{CG} = 1/4$, i.e., $k_{CG} = 8\pi$. (c) and (d): $r_{CG} = 1/16$, i.e., $k_{CG} = 32\pi$. (e) and (f): $r_{CG} = 1/64$, i.e., $k_{CG} = 128\pi$. (a), (c) and (e): to kinetic energy $T_{\mathcal{K}}^{(4)}(\mathbf{x})$, and (b), (d) and (f): to stretching energy $T_S(\mathbf{x})$.

tween $T_{\mathcal{K}}^{(4)}(\mathbf{x})$ and $T_S(\mathbf{x})$ are large for all scales as recognized from color distribution. It suggests that the energy transfer through boundaries of A is small as expected.

To quantify the scale-dependence of the above correlation, the correlations between energy transfers defined by

$$C(r_{CG}; T_X, T_Y) = \frac{\langle (T_X - \langle T_X \rangle)(T_Y - \langle T_Y \rangle) \rangle}{\sqrt{\langle (T_X - \langle T_X \rangle)^2 \rangle \langle (T_Y - \langle T_Y \rangle)^2 \rangle}} \quad (25)$$

are shown in Fig. 11, where T_X and T_Y are coarse-grained field of T_X and T_Y with the scale r_{CG} , respectively. Here, $\langle \cdot \rangle$ represents averaging over space and ensembles.

Only two combinations of energy transfers, namely $(T_{\mathcal{K}}^{(2)}, T_B)$ and $(T_S, T_{\mathcal{K}}^{(4)})$, show large correlation and its scale-dependence clearly. These correlations are negative and decrease toward -1 as the coarse-grained scale become large. The absolute values of correlations at the moderate phases are larger than those at the active phases, which might be understood by recalling the fact

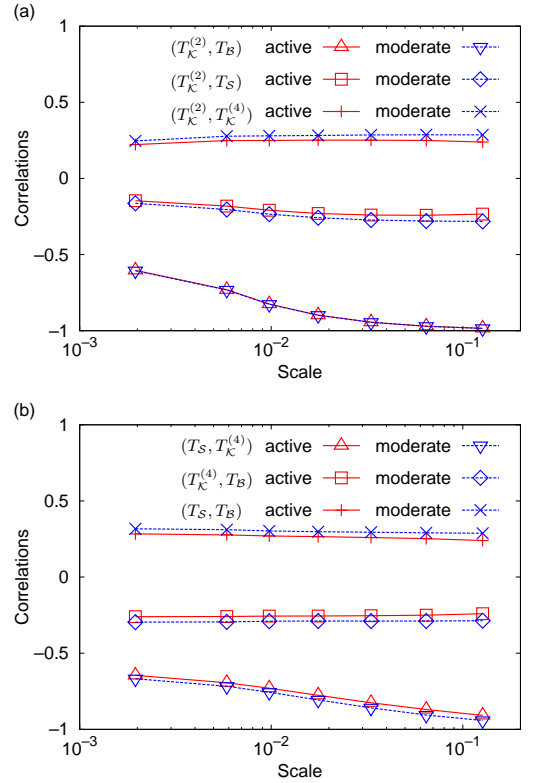


FIG. 11. (Color online) Scale dependence of the correlations between energy transfers.

that the interactions among different scales are larger at the active phases.

It might be interesting to point out that the correlation between linear energy transfers $(T_{\mathcal{K}}^{(2)}, T_B)$ approaches -1 with increasing scales faster than the one between nonlinear energy transfers $(T_S, T_{\mathcal{K}}^{(4)})$. The coexistence of the weak turbulence and the strong turbulence has been reported in the previous papers [4, 7, 8]; the weak turbulence in the small scales, i.e., the large wave numbers, and the strong turbulence in the large scales, i.e., the small wave numbers. In other words, the energy transmutation between the kinetic energy and the bending energy via $(T_{\mathcal{K}}^{(2)}, T_B)$ is active in both weak and strong turbulence, while the energy transfer between the kinetic energy and the stretching energy via $(T_S, T_{\mathcal{K}}^{(4)})$ is mainly in the strong turbulence.

V. SUMMARY

We have numerically analyzed the energy transfers in the statistically-steady non-equilibrium state in elastic-wave turbulence. We have focused on the nonlinear kinetic-energy transfer $T_{\mathcal{K}}^{(4)}$ and the nonlinear stretching-energy transfer T_S , since the energy transfers among different scales occur only through the exchange between the kinetic energy and the stretching energy as reported

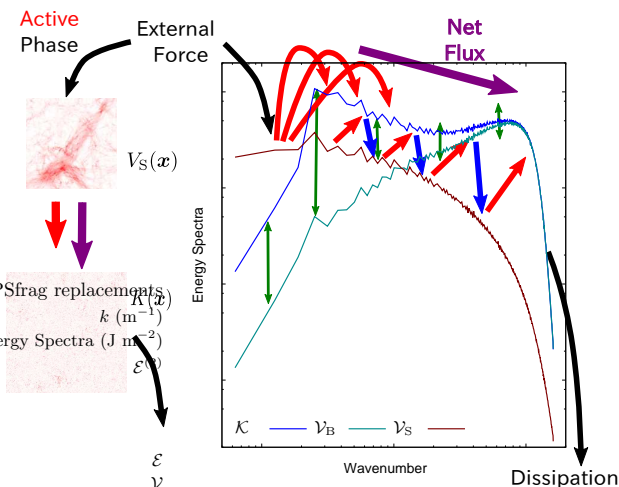


FIG. 12. (Color online) Schematic representation of energy transfers.

in Ref. [4]. In other words, the analytical expression of the energy transfers declares that the wave-number modes of the bending energy are only a mediator in the triad interaction. We have successfully visualized the energy transfer through a triad interaction, and hence the transfer between the kinetic energy of a wave-number mode and the stretching energy of another wave-number mode by using the analytical expression of the detailed energy balance among three wave-number modes. The local and nonlocal interactions of energy transfers can be recognized. The nonlocality of the net energy transfers in the strong turbulence has been found. The energy transfers from or to the representative scales were shown, and they reveal the distinctive configuration of the interactions in each scale of the forcing, strong-turbulence, weak-turbulence, and dissipation ranges.

By using the time variation of the systems's nonlinearity, the energy transfers were investigated separately in the active and moderate phases. At the active phases, the bundles of fibrous structures and the point-like struc-

tures emerge in the real space, and these intermittent real-space structures cause a large amount of the energy transfer in the Fourier space then. At the moderate phase, no such strongly nonlinear structures have been observed, and the energy transfers are caused mainly by the weakly nonlinear interactions of elementary waves as described in the weak turbulence theory.

In Fig. 12, we have schematically obtained an integrated picture of the energy transfers in the elastic-wave turbulence maintained by large-scale forcing. The external force gives energy to the forced wave numbers as its stretching energy at the active phase. In the real space, the strongly-nonlinear intermittent bundle structures are created at the active phase. The intermittent structures distribute the energy to the wave numbers in the strong turbulence through the nonlocal interactions in the Fourier space. The locally-cascading interactions between the kinetic and stretching energies also transfers energy to the large wave numbers. In the weak turbulence, the energy transfer due to the nonlocal interactions vanishes, and the weakly-nonlinear resonant interactions according to the weak turbulence theory, which are local in the Fourier space, play a dominant role. After the energy is transferred to the dissipation range, the energy is dissipated from the kinetic energy. The nonlocal interactions due to the intermittent structures and the locally-cascading interactions between the kinetic and stretching energies make the net energy flux to the large wave numbers. The bending energy mediates the energy transfer in the nonlinear interactions, and it is directly involved only in the linear transmutation between the kinetic energy and the bending energy.

ACKNOWLEDGMENTS

Numerical computation in this work was carried out using the computer facilities at the Yukawa Institute, Kyoto University and Research Institute for Information Technology, Kyushu University. This work was partially supported by KAKENHI Grant No. 15K17971, No. 16K05490 and No. 17H02860.

-
- [1] A. N. Kolmogorov, Dokl. Akad. Nauk SSSR **434**, 16 (1941).
 - [2] J. A. Domaradzki and R. S. Rogallo, Phys. Fluids A **2**, 413 (1990); F. Waleffe, *ibid.* **4**, 350 (1992); K. Ohkitani, *ibid.* **2**, 1529 (1990).
 - [3] K. Ohkitani and S. Kida, Phys. Fluids A **4**, 794 (1992).
 - [4] N. Yokoyama and M. Takaoka, Phys. Rev. E **90**, 063004 (2014).
 - [5] G. Düring, C. Josserand, and S. Rica, Phys. Rev. Lett. **97**, 025503 (2006).
 - [6] N. Mordant, Phys. Rev. Lett. **100**, 234505 (2008); A. Boudaoud, O. Cadot, B. Odille, and C. Touzé, *ibid.* **100**, 234504 (2008).
 - [7] N. Yokoyama and M. Takaoka, Phys. Rev. Lett. **110**, 105501 (2013).
 - [8] N. Yokoyama and M. Takaoka, Phys. Rev. E **89**, 012909 (2014).
 - [9] S. Sridhar and P. Goldreich, Astrophys. J. **432**, 612 (1994).
 - [10] S. Nazarenko, *Wave Turbulence* (Springer, Heidelberg, 2011); R. Bedard, S. Lukaschuk, and S. Nazarenko, "Gravity wave turbulence in a large flume," in *Advances in Wave Turbulence* (World Scientific, 2013) pp. 187–237.
 - [11] B. Miquel, A. Alexakis, and N. Mordant, Phys. Rev. E **89**, 062925 (2014).
 - [12] M. Onorato, S. Residori, U. Bortolozzo, A. Montina, and

- F. T. Arecchi, Phys. Rep. **528**, 47 (2013).
- [13] P. A. E. M. Janssen, J. Phys. Oceanogr. **33**, 863 (2003).
- [14] T. A. Witten, Rev. Mod. Phys. **79**, 643 (2007).
- [15] B. Miquel, A. Alexakis, C. Josserand, and N. Mordant, Phys. Rev. Lett. **111**, 054302 (2013).
- [16] S. Chibbaro and C. Josserand, Phys. Rev. E **94**, 011101 (2016).
- [17] L. D. Landau and E. M. Lifshitz, *Theory of Elasticity* (Butterworth–Heinemann, Oxford, 1986).
- [18] B. Audoly and Y. Pomeau, *Elasticity and geometry* (Oxford University Press, Oxford, 2010).
- [19] D. J. Webb, Deep Sea Res. **25**, 279 (1978).
- [20] K. Ohkitani, Phys. Fluids A **2**, 1529 (1990); J.-P. Laval, B. Dubrulle, and S. Nazarenko, Phys. Rev. Lett. **83**, 4061 (1999).